

Investigation of a non-Hermitian edge burst with time-dependent perturbation theory

Pengyu Wen,^{1,*} Jinghui Pi^{1,*},[†] and Gui-Lu Long^{1,2,3,‡}

¹*Department of Physics, Tsinghua University, Beijing 100084, China*

²*Frontier Science Center for Quantum Information, Beijing 100084, China*

³*Beijing Academy of Quantum Information Sciences, Beijing 100193, China*



(Received 6 April 2023; revised 7 November 2023; accepted 5 February 2024; published 26 February 2024)

Edge burst is a phenomenon in non-Hermitian quantum dynamics discovered by a recent numerical study [Phys. Rev. Lett. **128**, 120401 (2022)]. It finds that a large proportion of particle loss occurs at the system boundary in a class of non-Hermitian quantum walk. In this paper, we investigate the evolution of real-space wave functions for this lattice system. We find the wave function of the edge site is distinct from the bulk sites. Using time-dependent perturbation theory, we derive the analytical expression of the real-space wave functions and find that the different evolution behaviors between the edge and bulk sites are due to their different nearest-neighbor site configurations. We also find the edge wave function primarily results from the transition of the two nearest-neighbor nondecay sites. Besides, the numerical diagonalization shows the edge wave function is mainly propagated by a group of eigenmodes with a relatively large imaginary part. Our work provides an analytical method for studying non-Hermitian quantum dynamical problems.

DOI: [10.1103/PhysRevA.109.022236](https://doi.org/10.1103/PhysRevA.109.022236)

I. INTRODUCTION

The Hermiticity of the Hamiltonian is a fundamental requirement for a closed system in quantum physics [1]. In many situations, however, one is only interested in a limited subspace of the whole system, and it can be encapsulated in an effective non-Hermitian Hamiltonian [2,3]. Such systems include but are not limited to optical systems with gain and loss [4–14], open systems with dissipation [15–22], and electron systems with finite-lifetime quasiparticles [23–28]. Another important class of non-Hermitian systems is provided by lattices, where the role of topology has attracted tremendous interest [29–115]. A unique feature of non-Hermitian lattices is the non-Hermitian skin effect (NHSE), namely, the localization of an enormous number of bulk-band eigenstates at the edges under open boundary conditions [35–39,59–61,73,89–93]. A significant consequence of the NHSE is the breakdown of the conventional bulk-boundary correspondence, which can be recovered by using the localized skin modes replacing the extended Bloch waves of Hermitian lattices [33–35,43,76–78,83]. It indicates that the boundary is even more important in non-Hermitian physics compared with their Hermitian counterparts.

Recently, a novel boundary-induced dynamical phenomenon named “edge burst” is reported in Ref. [116] and an experimental verification is reported in Ref. [117]. When a quantum particle (called “quantum walker”) walks freely in a class of lossy lattices, it is intuitively expected that the decay probability is dominated by the lossy sites near the initial

location of the walker. Surprisingly, the numerical study finds that there is an unexpected remarkable loss probability peak at the edge, with an almost invisible loss probability tail in the bulk [116]. The appearance of such an edge peak has also been reported in an earlier work with an incorrect explanation [84], which is based on topology. The edge burst was regarded as an interplay of the NSHE and the imaginary gap closing in Ref. [116], where the authors give a criterion based on the property of the Hamiltonian. Although previous work has investigated the edge burst phenomenon, however, the relation between the real-space dynamical behavior of the system and the formation of this burst edge lossy peak is still unknown.

In this work, we investigate the real-space dynamical behavior of quantum particles in a lossy lattice. Numerical simulations show the edge burst phenomenon is closely related to the distinct dynamical behaviors of wave functions between the edge and bulk sites. To further understand how the walker propagates in the lattice, we introduce time-dependent perturbation theory in non-Hermitian systems and evaluate the analytical expression of the real-space quantum walk wave functions. Due to the NHSE, the walker mainly hops nonreciprocally along the nondecay chain. The analysis of real-space wave functions shows the different evolution features between the edge and bulk can be attributed to their nearest-neighbor site configurations, which limits the possible path the walker can travel from the initial state. Besides, we find that the main contribution to the edge wave function originates from the interference transition of the two nearest-neighbor nondecay sites. Furthermore, we discuss the relation between the evolution of the system and its open (periodic) boundary eigenmodes by numerical diagonalization. The result shows the walker is mainly propagated by a group of eigenmodes which have a large imaginary part when it arrives at the edge. Our work gives an explicit illustration of the edge

*These authors contributed equally to this work.

[†]pijh14@gmail.com

[‡]gllong@tsinghua.edu.cn

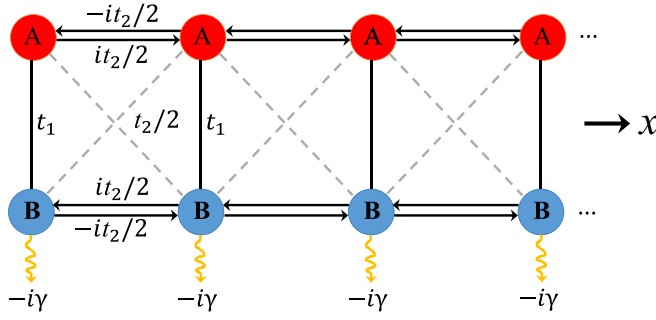


FIG. 1. Schematic diagram of the non-Hermitian lattice. Each unit cell, labeled by spatial coordinate x , contains two sites A and B.

burst phenomenon in real space and provides an alternative method to investigate non-Hermitian dynamical problems.

This paper is organized as follows: We introduce the non-Hermitian quantum walk model and describe the edge burst phenomenon with numerical simulations in Sec. II. A sketch of the time-dependent perturbation theory for a non-Hermitian Hamiltonian is given in Sec. III. We apply the theory in a concrete quantum walk model and solve the evolution equation analytically in Sec. IV. By the analysis of wave functions, we elucidate the propagation process of the walker and the formation of edge burst in real space directly. In Sec. V, we discuss the relation between the evolution of the edge wave function and the eigenstates of the system. Finally, a summary and discussion are given in Sec. VI.

II. MODEL AND NON-HERMITIAN EDGE BURST

Let us consider a one-dimensional non-Hermitian lattice (see Fig. 1), from which the walker can escape during the quantum walk. The state of the system $|\psi\rangle$ evolves according to the following equations of motion (we set $\hbar = 1$):

$$\begin{aligned} i\frac{d\psi_x^A}{dt} &= t_1\psi_x^B + i\frac{t_2}{2}(\psi_{x-1}^A - \psi_{x+1}^A) + \frac{t_2}{2}(\psi_{x-1}^B + \psi_{x+1}^B), \\ i\frac{d\psi_x^B}{dt} &= t_1\psi_x^A - i\frac{t_2}{2}(\psi_{x-1}^B - \psi_{x+1}^B) + \frac{t_2}{2}(\psi_{x-1}^A + \psi_{x+1}^A) \\ &\quad - i\gamma\psi_x^B, \end{aligned} \quad (1)$$

where $\psi_x^A = \langle x, A|\psi\rangle$ and $\psi_x^B = \langle x, B|\psi\rangle$ are the amplitudes of the walker on the sublattices A and B at the site x . Without loss of generality, we choose the hopping amplitude parameters t_1 and t_2 to be real numbers. The onsite imaginary potential $-i\gamma$ describes the loss particles on B sites with rate 2γ . This model differs from the previous quantum walk model [7], as it features the NHSE. This can be seen clearly by mapping a similar model in Ref. [29], to the non-Hermitian Su-Schrieffer-Heeger (SSH) model with nonreciprocal hopping [35]. The mathematical relation of these lattice models can be seen in Appendix A.

For a general Hamiltonian $\hat{\mathcal{H}} = \hat{H} - i\hat{\Gamma}$, where \hat{H} and $\hat{\Gamma}$ are Hermitian operators, the norm of a quantum state $|\psi\rangle$ evolves according to $\frac{d}{dt}\langle\psi|\psi\rangle = -2\langle\psi|\hat{\Gamma}|\psi\rangle$. In the non-Hermitian quantum walk model we consider, the system decays according to $\frac{d}{dt}\langle\psi|\psi\rangle = -\sum_x 2\gamma|\psi_x^B|^2$, and the local

decay probability on site x is

$$P_x = \int_0^\infty 2\gamma|\psi_x^B(t)|^2 dt. \quad (2)$$

If the initial state $|\psi(0)\rangle$ is normalized, the decay probability distribution satisfies $\sum_x P_x = 1$. Now, suppose a walker starts from some sublattice A of site x at time $t = 0$, namely, $\psi_x^A(0) = \delta_{x,x_0}$, $\psi_x^B(0) = 0$, and involves freely under the equations of motion (1). The hop between different sites drive the walker away from x_0 , and during this quantum walk, the walker can escape from any B sites. This can be seen clearly in Figs. 2(a) and 2(b), which is the numerical solution of P_x . The distribution of P_x is left-right asymmetric and it originates from the NSHE, the walker tends to jump towards the left as all eigenstates are localized at the left edge.

A fascinating property of the system is the edge burst [116], namely, the appearance of a prominent peak in the loss probability at the edge, with the nearby almost invisible decaying tail [see Fig. 2(a)]. Such an unexpected peak was numerically seen in the earlier Ref. [84] and was attributed to topological edge states. This interpretation was regarded as wrong in Ref. [116] for the disappearance of the high peak in the topological nontrivial region. To explore how the walker propagates in the lattice and forms a burst loss probability peak at the edge, we focus on the time evolution of ψ_x^B . The numerical result shows that ψ_x^B are purely imaginary. Furthermore, when there is the edge burst phenomenon, the dynamical evolution of wave function at the edge is distinct from the bulk one. We can see this clearly in Fig. 2(c) that ψ_1^B has a tremendous large increased amplitude peak after the first tiny peak, while other $\psi_{x\neq 1}^B$ oscillate with a decreasing amplitude as t becomes larger. This interesting feature is crucial to form a burst edge peak. There is no such tremendous large increased peak for ψ_1^B in Fig. 2(d), where all ψ_x^B have the same decreased oscillation behavior, and the corresponding edge loss probability P_1 in Fig. 2(b) is very small.

III. NON-HERMITIAN TIME-DEPENDENT PERTURBATION THEORY

The analytical expression of $\psi_x^B(t)$ can be obtained via time-dependent perturbation theory. The sketch of this theory is encapsulated as follows: We consider a non-Hermitian Hamiltonian $\hat{H}(t)$ such that it can be split into time-independent part \hat{H}_0 and time-dependent part $\hat{H}'(t)$, namely,

$$\hat{H}(t) = \hat{H}_0 + \hat{H}'(t). \quad (3)$$

The corresponding Schrödinger equation is

$$i\frac{\partial}{\partial t}|\Psi(t)\rangle = \hat{H}(t)|\Psi(t)\rangle. \quad (4)$$

When $\hat{H}'(t) = 0$, Eq. (4) can be solved if we know the solution of eigenequations $\hat{H}_0|n\rangle = E_n|n\rangle$ with eigenstates $|n\rangle$ and eigenvalues E_n , that is

$$|\Psi(t)\rangle = e^{-i\hat{H}_0 t}|\Psi(0)\rangle, \quad (5)$$

where $|\Psi(0)\rangle$ is the linear combination of $|n\rangle$. If $\hat{H}'(t) \neq 0$, it is no longer a stationary problem and we are interested in the case that the initial state $|k\rangle$ is one of the eigenstates

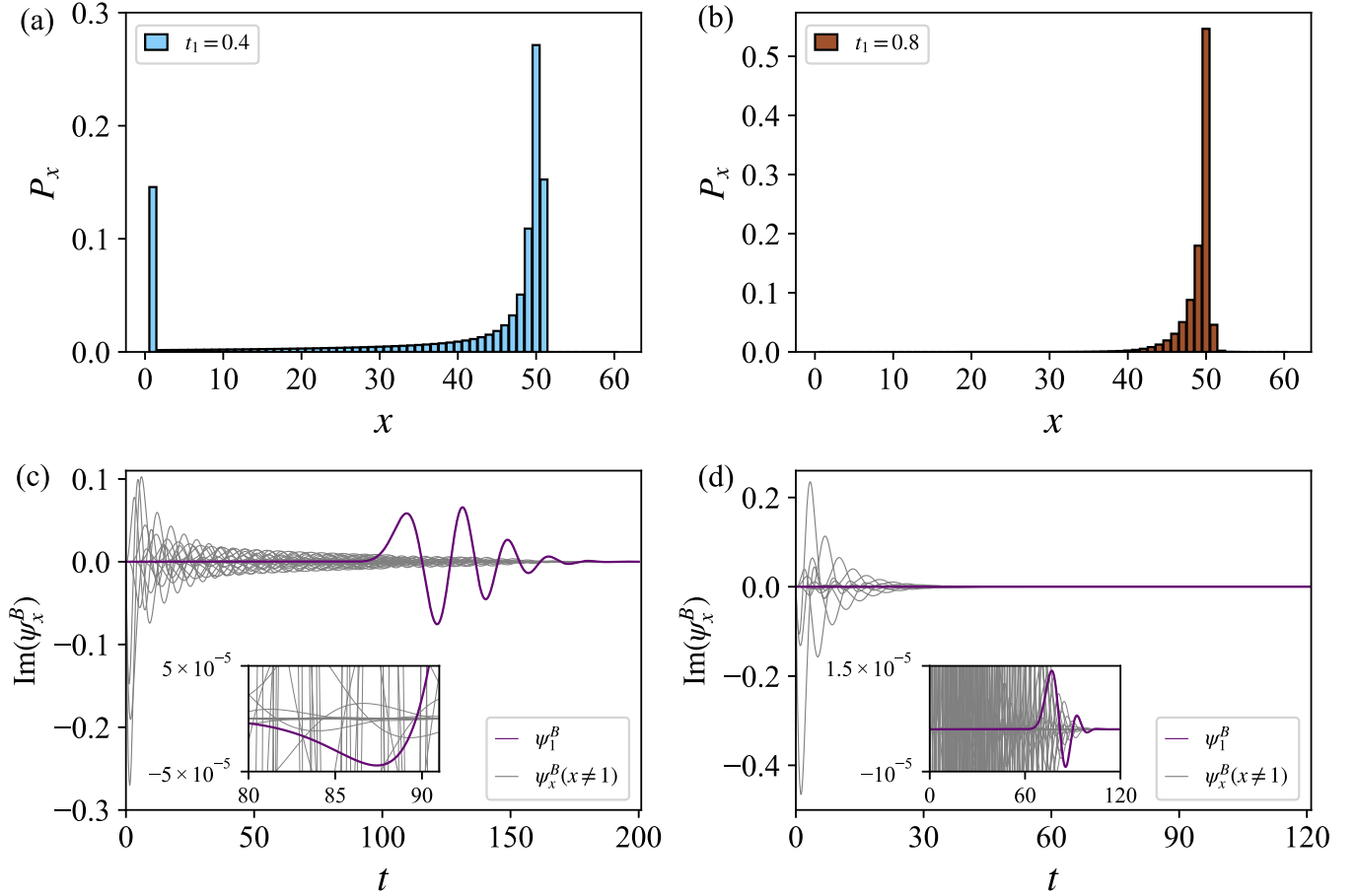


FIG. 2. (a), (b) The spatially resolved loss probability P_x for a walker initiated at $x_0 = 50$. $t_1 = 0.4$ for panel (a) and $t_1 = 0.8$ for panel (b). The chain length $L = 60$. (c), (d) The corresponding time evolution of ψ_x^B to panels (a) and (b) respectively. The common parameters $t_2 = 0.5$ and $\gamma = 0.8$ are fixed throughout panels (a)–(d).

of \hat{H}_0 . Due to the perturbation of $\hat{H}'(t)$, the state $|k\rangle$ is an unstable state. We assume the system is a superposition of the eigenstates of \hat{H}_0 for $t > 0$ and given by

$$|\Psi(t)\rangle = \sum_n |\psi_n(t)\rangle = \sum_n c_n(t) e^{-iE_n t} |n\rangle. \quad (6)$$

Substituting this ansatz wave function into Schrödinger equation (4) and multiplying by the state $\langle m|$, we get a coupled differential equation of wave function expansion coefficient under unperturbed representation \hat{H}_0 :

$$i \frac{dc_m(t)}{dt} = \sum_n H'_{mn}(t) c_n(t) e^{i(E_m - E_n)t}, \quad (7)$$

where $H'_{mn}(t) = \langle m|\hat{H}'(t)|n\rangle$. To solve the differential equation (6) with the initial condition $c_m(0) = \delta_{mk}$, we take the perturbation expansion of $c_m(t)$ and use the iteration method. Specifically, $c_m(t)$ can be written as

$$c_m(t) = c_m^{(0)} + c_m^{(1)} + c_m^{(2)} + \dots, \quad (8)$$

where $c_m^{(1)}, c_m^{(2)}, \dots$ signify amplitudes of the first order, second order, and so on in the strength parameter of time-dependent Hamiltonian. Plugging Eq. (8) into Eq. (7) and comparing the order of perturbation, we can get the l th-order

equation:

$$i \frac{d}{dt} c_m^{(l)}(t) = \sum_n H'_{mn}(t) c_n^{(l-1)}(t) e^{i(E_m - E_n)t}. \quad (9)$$

This equation can be solved easily by integrating it directly if we know all of $(l-1)$ st-order solutions $c_n^{(l-1)}$. Thus, we can solve Eq. (7) step by step, and the solution up to l th-order is

$$c_m(t) \simeq c_m^{(0)}(t) + c_m^{(1)}(t) + \dots + c_m^{(l)}(t). \quad (10)$$

It should be noticed that this approximate solution has a convergent radius t_0 , which is related to the perturbation expansion order and the strength parameters of perturbation.

IV. BURST PEAK FROM TIME-DEPENDENT PERTURBATION THEORY

In the non-Hermitian quantum walk model, the onsite potential operator is set as the unperturbed Hamiltonian \hat{H}_0 . Its real-space matrix elements are $\langle x, s|\hat{H}_0|x', s'\rangle = -\frac{i\gamma}{2} \delta_{xx'} \delta_{ss'} [1 - (\sigma_z)_{ss'}]$, where x, x' referring to the location of the unit cell and $s, s' = A, B$ referring to the sublattice label. The eigenequation is $\hat{H}_0|x, s\rangle = E_x^s|x, s\rangle$, with two N -fold eigenvalues $E_x^A = 0$ and $E_x^B = -i\gamma$, respectively. The hopping of the walker is treated as the perturbation operator \hat{H}' and its matrix elements are $H'_{xx', s's'} = \langle x, s|\hat{H}'|x', s'\rangle$. Thus,

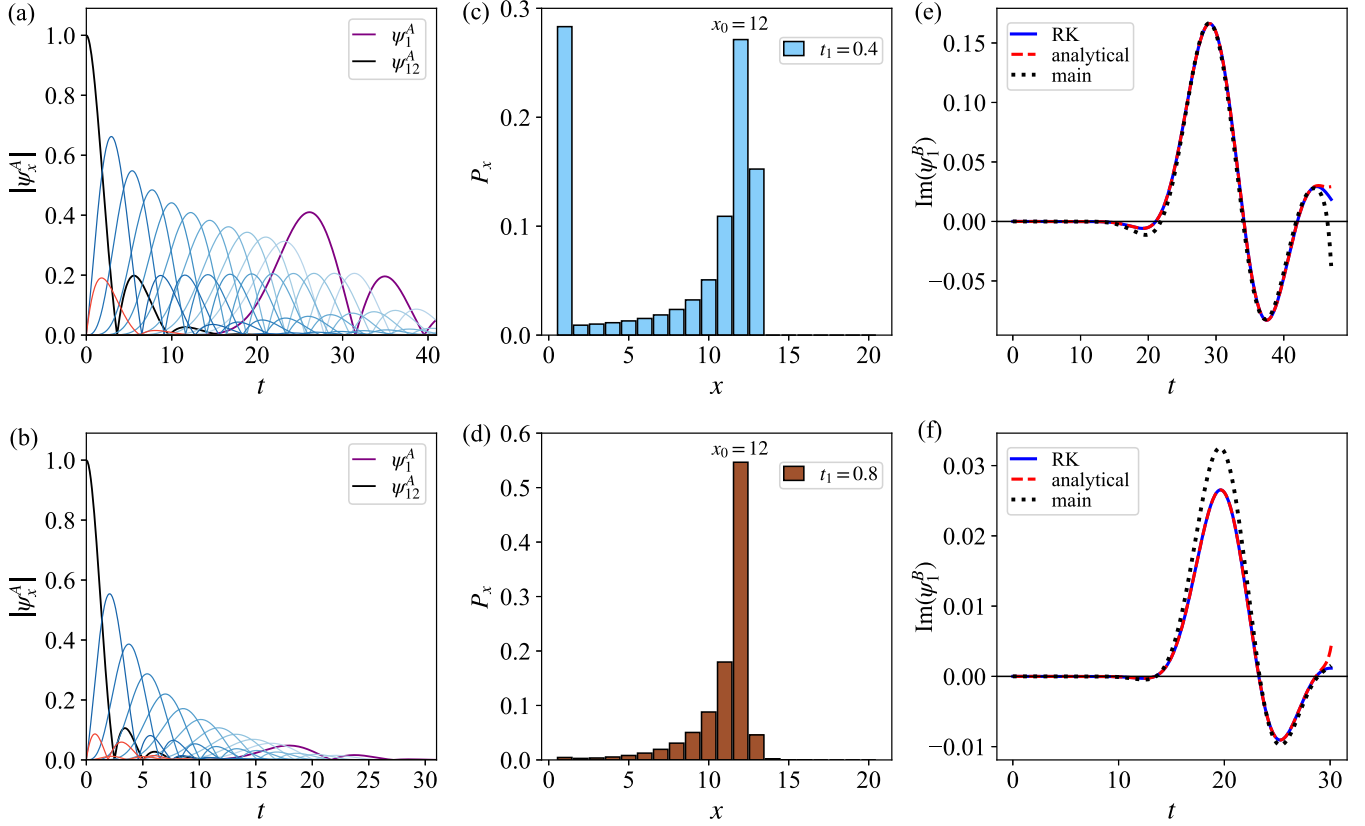


FIG. 3. (a), (b) The modulus of the wave functions $\psi_x^A(t)$ for a walker initiated at $x_0 = 12$. $t_1 = 0.4$ for panel (a) and $t_1 = 0.8$ for panel (b). The gradient blue (red) curves represent the sites that are on the left (right) side of the initial site, namely, from $|\psi_{11}^A(t)|$ to $|\psi_{20}^A(t)|$ [$|\psi_{13}^A(t)|$ to $|\psi_{20}^A(t)|$]. The lighter the blue (red) color of the curve is, the further the site is away from the initial site. Specifically, the black curve represents the initial 12A site while the purple curve represents the left edge site 1A. The chain length $L = 20$. (c), (d) The corresponding spatially resolved loss probability P_x to panels (a), (b) respectively. Panels (e) and (f) are the edge wave functions $\psi_x^B(t)$. The blue solid line means the Runge-Kutta numerical solution. The evaluation of both analytical (red dashed) and main paths (black dotted) are up to 90th-order perturbation. The common parameters $t_2 = 0.5$ and $\gamma = 0.8$ are fixed throughout panels (a)–(f).

according to the perturbation procedure in Sec. III, we can evaluate the evolution of the amplitude of the walker on any site. Specifically, Eq. (7) will be reduced to

$$i \frac{dc_x^s(t)}{dt} = \sum_{x's'} H'_{xs,x's'} c_{x'}^{s'}(t) e^{i(E_x^s - E_{x'}^{s'})t}. \quad (11)$$

One can integrate both sides of this equation and get the formal solution,

$$c_x^s(t) = -i \sum_{x's'} \int_0^t H_{xs,x's'} c_{x'}^{s'}(t') e^{i(E_x^s - E_{x'}^{s'})t'} dt'. \quad (12)$$

with the relation $\psi_x^s(t) = e^{-iE_x^s t} c_x^s(t)$, the formal solution can be written as the relation between the amplitude of the different sites:

$$\psi_x^s(t) = -ie^{-iE_x^s t} \sum_{x's'} \int_0^t e^{iE_{x'}^{s'} t'} H_{xs,x's'} \psi_{x'}^{s'}(t') dt'. \quad (13)$$

Initial conditions $\psi_x^A(0) = \delta_{x,x_0}$ and $\psi_x^B(0) = 0$ guarantee that the amplitudes $\psi_x^A(t)$ remain real and $\psi_x^B(t)$ remain purely imaginary for all t . This follows from the perturbation analysis (see details in Appendix B). Alternatively, one can check this conclusion through the iteration equation (13). For example,

if the sublattice label $s = A$, the nonzero factors $H_{xs,x's'} \psi_{x'}^{s'}(t')$ are imaginary under the assumption that $\psi_{x'}^{s'}(t')$ are real for $s' = A$ and imaginary for $s' = B$. The amplitudes $\psi_x^A(t)$ thus keep real, which is a self-consistent result for equation (13).

For concreteness, we consider a 20-site lattice with the walker initially prepared on sublattice A of site 12. Analytical expressions of wave functions $\psi_x^s(t)$ are obtained using time-dependent perturbation theory, and these expressions agree well with the numerical results at the desired time. It finds that the dynamical behavior of the walker along the A chain is crucial to forming a remarkable loss peak at the edge. Increasing the hopping parameter t_1 strengthens the coupling between chains A and B for fixed t_2 and γ , thereby accelerating walker dissipation and consequently shortening its travel time on chain A. This manifests in Figs. 3(a) and 3(b), where $\psi_x^A(t)$ exhibits smaller amplitudes and faster convergence to zero for larger t_1 upon the walker's arrival at x . Another perspective to see this is that the dissipation probabilities P_x near the initial location is larger as t_1 increases [see Figs. 3(c) and 3(d)]. If the system satisfies the imaginary gapless condition $t_1 < t_2$, the walker will decay slowly with the algebraic behavior of bulk P_x [96,116], which leads a large amplitude of ψ_1^A [see Fig. 3(a)]. On the other hand, this non-Hermitian lattice model

features the NHSE, namely, the exponential localization of all eigenstates at the edge, which is characterized by the generalized Bloch factor β with $|\beta| = \sqrt{|(t_1 - \gamma/2)/(t_1 + \gamma/2)|}$. In the case $|\beta| < 1$ for $t_1 > 0$, all skin modes are localized at the left edge. The NHSE induces leftward walking along the A chain with $\max[|\psi_{x < x_0}^A|]$ much larger than $\max[|\psi_{x > x_0}^A|]$, as shown in Figs. 3(a) and 3(b). The walker becomes trapped at the left edge once it arrives at A_1 , which leads to the Rabi-like oscillation between sublattice A_1 and B_1 . With such a Rabi-like oscillation picture in mind, one can easily combine the prominent burst of the purple $|\psi_1^A(t)|$ curve in Fig. 3(a) with the dissipation probability burst in B_1 in Fig. 3(c). A larger $|\psi_1^A(t)|$ will result in a larger amplitude of the quantum jump $|1, A\rangle \rightarrow |1, B\rangle$.

The complete analytical expression of $\psi_x^s(t)$ can be interpreted as the sum of all physically allowed paths the walker traverses from $|x_0, A\rangle$ to $|x, s\rangle$ during time t . For example, the walker can reach $|x_0, B\rangle$ via only one single-step quantum jump from $|x_0, A\rangle$, while four distinct paths exist for a two-step jump. These paths correspond to the first- and second-order perturbation contributions in $\psi_{x_0}^B(t)$, respectively. We can classify every perturbation process by its final-step quantum jump. The sum of all perturbation terms with the same final-step quantum jump is the total transition amplitude from a certain nearest-neighbor site of $|x, s\rangle$ to $|x, s\rangle$. This is the physical interpretation of the integral formula (13). When the walker travels from $|x_0, A\rangle$ to $|x, s\rangle$ for a bulk site x , there are five transition process, corresponding to five final step quantum jumps $|x', s'\rangle \rightarrow |x, s\rangle$ with $s' = A, B$ for $x' = x \pm 1$ and $s' \neq s$ for $x' = x$. However, the number of different final step quantum jumps is reduced to three if the walker arrives at $x = 1$. This feature leads the nonzero hopping matrix element $H_{x's, x's'}$ in equation (13) to be five for the bulk x and three for the edge one. Thus, the contrasting evolution of bulk and edge wave functions in the edge burst phenomenon originates from their distinct nearest-neighbor site configurations. These configurations constrain the permissible paths a walker can travel from the initial state. For example, a quantum jump process $|x + 1, A\rangle \rightarrow |x, B\rangle \rightarrow |x - 1, A\rangle \rightarrow |x, B\rangle$ is allowed in the bulk sites but forbidden in the edge site. Another perspective to see this is that if we neglect the back transition from the two forward nearest-neighbor sites, the bulk wave function evolves like the edge wave function as it can be viewed as the new physical edge artificially. Furthermore, we find that the edge wave function $\psi_1^B(t)$ can be approximated by the interference of transition amplitude from two adjacent nondecay sites A_1 and A_2 , or symbolically,

$$\psi_1^B(t) \simeq -ie^{-\gamma t} \int_0^t e^{\gamma t'} \left[t_1 \psi_1^A(t') + \frac{t_2}{2} \psi_2^A(t') \right] dt'. \quad (14)$$

Figures 3(e) and 3(f) visually confirm this, as we viewed the transition paths with final step quantum jumps A_1 to B_1 or A_2 to B_1 as the main paths, which fit well with analytical and Runge-Kutta numerical results. The reason is that the walker mainly propagates along the A chain and the transition amplitude from the B_2 site can be neglected as $\psi_2^B(t)$ is very small. Compared with the previously mentioned Rabi-like oscillation between A_1 and B_1 , a more accurate picture can be drawn

now. The walker starts from the initial site and propagates with a preference to the left due to the NHSE. After its arrival on site 2, the walker oscillates in an approximately closed loop formed by A_1 , A_2 , and B_1 until the particle finally decays out in B_1 . B_2 can be excluded out of the loop since $\psi_2^B(t)$ is very small. In the edge burst region, both $\psi_1^A(t)$ and $\psi_2^A(t)$ are relatively large as demonstrated in Fig. 3(a). Whereas they are fairly small in the region without edge burst as shown in Fig. 3(b).

The above discussions are all based on the initial condition that the walker starts from some sublattice A . However, we note that the initial condition is also crucial for the formation of the prominent loss peak at the edge. One can easily check that the edge loss peak is too small to be observed for the initial case that the walker starts from sublattice B even though the system features the NSHE and imaginary gap closing. See the analysis of the effect of the initial site in Appendix C.

V. THE EIGENMODES AND THE EDGE WAVE FUNCTION

To investigate the role that different eigenstates play in the evolution process, we decompose the non-Hermitian Hamiltonian by the biorthogonal bases

$$\hat{H} = \sum_n E_n |n_R\rangle \langle n_L|, \quad (15)$$

where $|n_R\rangle$ and $\langle n_L|$ are the right and left eigenstates, respectively, satisfying biorthogonality $\langle m_L | n_R \rangle = \delta_{mn}$ and completeness $\sum_n |n_R\rangle \langle n_L| = \mathbb{I}$. For the non-Hermitian lattice we investigate, the state of the system evolves according to

$$|\psi(t)\rangle = e^{-i\hat{H}t} |\psi(0)\rangle, \quad (16)$$

where the initial state $|\psi(0)\rangle$ can be expressed by a superposition of $|n_R\rangle$

$$|\psi(0)\rangle = \sum_n a_n |n_R\rangle, \quad (17)$$

where a_n is determined by the linear equations

$$\psi_x^s(0) = \sum_n a_n \phi_{n,x}^s, \quad (18)$$

with $\phi_{n,x}^s \equiv \langle x, s | n_R \rangle$. Thus, we can rewrite the evolution equation (16) as

$$|\psi(t)\rangle = \sum_n e^{-iE_n t} a_n |n_R\rangle. \quad (19)$$

Since $E_n = \text{Re}(E_n) + i\text{Im}(E_n)$, we can rewrite the evolution equation (19) as

$$|\psi(t)\rangle = \sum_n e^{-i\text{Re}(E_n)t} e^{\text{Im}(E_n)t} a_n |n_R\rangle. \quad (20)$$

Focusing on evolution equation (20), the long time behavior of $|\psi(t)\rangle$ is determined by the eigenstates with relatively large imaginary parts of eigenvalues since the exponential factor in front of them decay more slowly. So the imaginary parts of the eigenvalues play an important role in the time evolution of the wave function. Specifically, one can verify that the imaginary part of any eigenvalue of the system is always negative

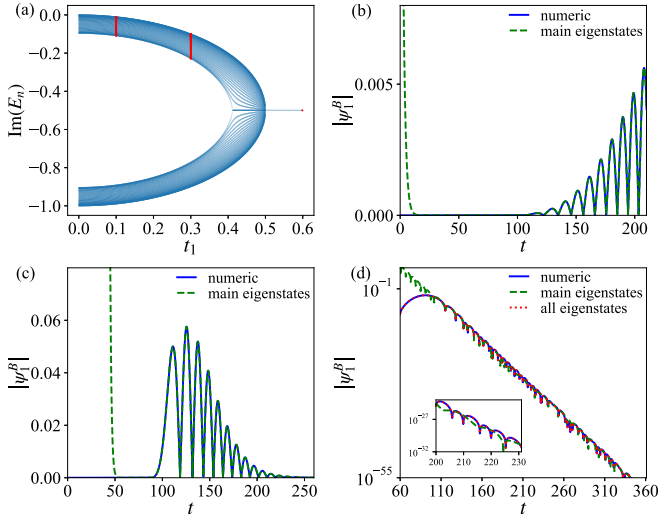


FIG. 4. (a) The imaginary part of energy E_n with $L = 60$. The red points at $t_1 = 0.1$, $t_1 = 0.3$, and $t_1 = 0.6$ correspond to the eigenstates we choose to simulate the time evolution of $|\psi_1^B(t)\rangle$. Other parameters are $t_2 = 0.4$, $\gamma = 1$ and the walker is initially put at site 40A. (b) The green dashed line represents the simulation by choosing 60 eigenstates with relatively large imaginary parts of eigenvalues. The blue solid line represents the Runge-Kutta numeric solution. $t_1 = 0.1$, other parameters are the same as in panel (a). (c) Similar to panel (b) except that $t_1 = 0.3$. (d) Similar to panel (b) except that $t_1 = 0.6$. The red dashed line represents the simulation of all 120 eigenstates, which exactly reveal the Runge-Kutta numerical solution.

owing to the dissipation of the whole system. Moreover, the imaginary part of the eigenvalues are twofold degenerate and symmetric to $-\frac{i}{2}\gamma$, which is demonstrated in Fig. 4(a). The reason is that the Hamiltonian of the quantum walk \hat{H} can be divided into two parts $\hat{H} = \hat{H}_1 - \frac{i\gamma}{2}\hat{I}$ with the first part \hat{H}_1 satisfying chiral symmetry and parity-time symmetry [29]. More details about the symmetry analysis of the Hamiltonian are given in Appendix A.

We still take a 60-site lattice as an example to show the role of the imaginary part of the eigenvalues play in the time evolution of the wave function. By picking 60 eigenstates with relatively large imaginary part of eigenvalues out of all 120 eigenstates, we fit the evolution of the wave function $|\psi_1^B(t)\rangle$ and show its result in Figs. 4(b)–4(d). For $t_1 = 0.1$, as one can see from the green dashed line in Fig. 4(b), these 60 eigenstates can describe the evolution of $|\psi_1^B(t)\rangle$ well as early as $t = 15$. This is because the other 60 eigenstates have much smaller imaginary parts of eigenvalues and their contribution to the wave function vanishes quickly. While in Fig. 4(c) with a different $t_1 = 0.3$, these 60 eigenstates can fit the analytical solution well only after $t = 50$, which is due to the non-negligible contribution of other 60 eigenstates before $t = 50$. When $t_1 = 0.6$, all eigenstates have the same imaginary part of the eigenvalues, which indicates that they contribute equally to the decay behavior of the wave function. If we still choose half of all eigenstates to fit the evolution of the wave function, the accurate simulation would fail even at a long-evolution time. Although the order of magnitude of the wave function

can be well described by half of the eigenstates after $t = 110$, the oscillation details are missed due to the exclusion of the other half of the eigenstates, which is demonstrated clearly in the green dashed line in the subfigure of Fig. 4(d). Apparently, the combination of all eigenstates can accurately restore the evolution of the wave function, which is shown in the red dashed line in Fig. 4(d).

The above discussions are all based on the imaginary part of the open boundary condition (OBC) spectrum $\{E_n\}$. Another perspective is to investigate the imaginary part of the periodic boundary condition (PBC) spectrum $\{E'_m\}$, which differs greatly from the OBC one due to the NHSE. For the dynamical evolution of the OBC system, one can also expand the wave function in the eigenstates of its PBC counterpart through a transform matrix T ,

$$|\psi(t)\rangle = \sum_m c_m(t)|m_k\rangle, \quad (21)$$

where $\{|m_k\rangle\}$ are the right eigenstates of the PBC Hamiltonian H_{PBC} with eigenvalue E'_m . One can easily find that the time-dependent coefficient $c_m(t)$ satisfies $c_m(t) = \sum_n T_{nm} e^{-iE'_n t} a_n$. Obviously, the module of $c_m(t)$ reveals the weight of the eigenstate $|m_k\rangle$ plays in the dynamical evolution. To investigate the relationship between the weight $|c_m(t)|$ and the imaginary part of the eigenvalue, $\text{Im}(E'_m)$, we plot the change of $|c_m(t)|$ over time in Fig. 5 for a 20-site system with the walker initialized at 15A. We have arranged $|c_m(t)|$ according to the magnitude of $\text{Im}(E'_m)$ in Fig. 5. The darker the color of the curve $|c_m(t)|$ is, the larger $\text{Im}(E'_m)$ is. One can easily tell that a larger $\text{Im}(E'_m)$ leads to $|c_m(t)|$ decays more slowly, which results in a larger integral area over t . The integral area of $|c_m(t)|$ over t can be viewed as another indicator of the weight of different eigenstates plays in the evolution process. By analyzing an OBC dynamical evolution problem with the PBC eigenstates and eigenvalues, we emphasize the importance of the imaginary part of the eigenvalues again, no matter whether the eigenvalues are OBCs or PBCs. Edge burst is an astonishing phenomenon in OBC. Herein, using the PBC quantity $|c_m(t)|$ to investigate an OBC dynamical problem may have some connection with the imaginary gap closing in Ref. [116], where the authors also set a PBC criterion of an OBC phenomenon.

VI. SUMMARY AND DISCUSSION

In this paper, we study the real-space dynamical evolution of quantum particles in the lossy lattices. We find the edge burst phenomenon is closely related to the distinct evolution features between the edge wave function and bulk wave functions by a numerical simulation. We then give a sketch of time-dependent perturbation theory for a non-Hermitian Hamiltonian and evaluate the analytical expression of the quantum walk wave function. Through the analysis of the perturbation solution, we find the walker mainly propagates nonreciprocally along the nondecay chain as the non-Hermitian lattices feature the NHSE. Moreover, the different evolution behaviors between the edge and bulk can be attributed to their nearest-neighbor site configurations, which limit the possible path that the walker can travel from the initial site. Besides, it finds that the main contribution to the

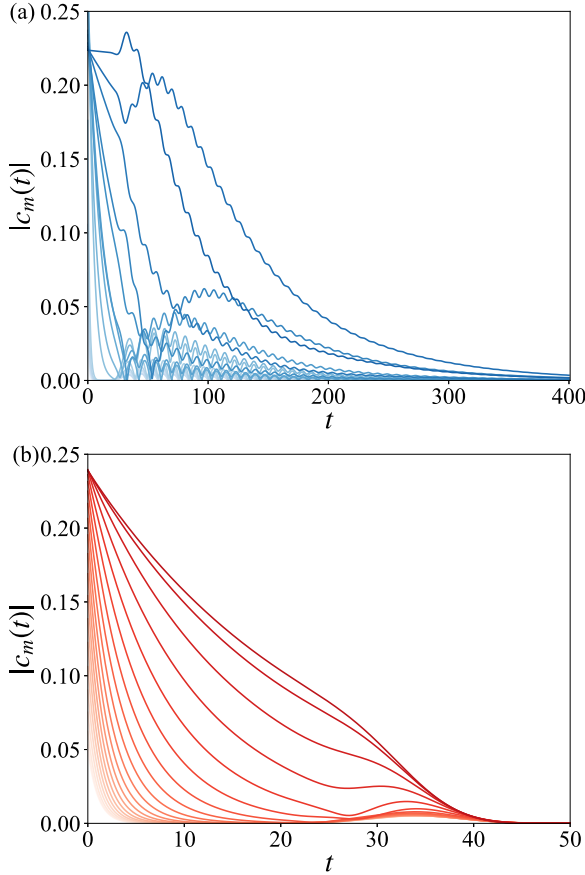


FIG. 5. The PBC eigenstates weight $|c_m(t)|$ versus t . The gradient color represents different $\{|c_m(t)|\}$ with different eigenvalues. The darker the color of the curve is, the larger the imaginary part of the eigenvalue is. One can tell that $|c_m(t)|$ with a larger imaginary part of the eigenvalue has a larger integral over t for both panels (a) and (b). (a) The edge burst region. $t_1 = 0.1$, $t_2 = 0.4$, $\gamma = 1$, the initial walker was put in 15A for a 20-site lattice. (b) The region without edge burst. Similar to panel (a) except for $t_1 = 0.6$.

edge wave function results from the interference transition of the two nearest-neighbor sites. Furthermore, the numerical diagonalization shows that the walker is mainly propagated by a group of eigenmodes that have a relatively large imaginary part.

Our work gives an explicit illustration of the edge burst phenomenon in real space directly and provides an alternative method to study this kind of non-Hermitian dynamical problem, for example, the quantum walk with a nonuniform loss rate [118] (details see Appendix D).

ACKNOWLEDGMENTS

The authors would like to thank Yumin Hu, Zheng Fan, and Yuting Lei for their helpful discussion. This work is supported by the National Natural Science Foundation of China under Grants No. 11974205 and No. 61727801, and the Key Research and Development Program of Guangdong Province (2018B030325002).

APPENDIX A: MATHEMATICAL RELATION BETWEEN SEVERAL LATTICE MODELS

In Appendix A, we mainly discuss the mathematical relation of lattice models mentioned in Sec. II. The Hamiltonian of the quantum walk model with N unit cell is

$$\hat{H} = \hat{H}_1 - \frac{i\gamma}{2} I_{2N \times 2N}, \quad (\text{A1})$$

where \hat{H}_1 has chiral symmetry and parity-time (\mathcal{PT}) symmetry [29]. The chiral symmetry is defined by $\Gamma = \bigoplus_n \sigma_y^n$, $\Gamma \hat{H}_1 \Gamma = -\hat{H}_1$ and the \mathcal{PT} symmetry is defined by $\mathcal{P} = \bigoplus_n \sigma_y^n$, $\mathcal{T} i \mathcal{T} = -i$, $\mathcal{PT} \hat{H}_1 \mathcal{T}^{-1} \mathcal{P}^{-1} = \hat{H}_1$. The Hamiltonian \hat{H}_1 can be transformed to the non-Hermitian SSH model with left-right asymmetric hopping by a $\pi/2$ rotation about the x -axis to each spin if we viewed every sublattice as a pseudospin, or symbolically,

$$\hat{H}_2 = \mathcal{R}^{-1} \hat{H}_1 \mathcal{R}, \quad (\text{A2})$$

where

$$\hat{H}_2 = \begin{bmatrix} 0 & t_1 + \frac{\gamma}{2} & 0 & 0 & \cdots \\ t_1 - \frac{\gamma}{2} & 0 & t_2 & 0 & \cdots \\ 0 & t_2 & 0 & t_1 + \frac{\gamma}{2} & \cdots \\ 0 & 0 & t_1 - \frac{\gamma}{2} & 0 & \ddots \\ \vdots & \vdots & \vdots & \ddots & \ddots \end{bmatrix}_{2N \times 2N}, \quad (\text{A3})$$

and the spin rotate operator is $\mathcal{R} = \bigoplus_n e^{-i\frac{\pi}{4}\sigma_x^n}$. The Hamiltonian \hat{H}_2 can also be related to the standard SSH model via a similarity transformation [35], or symbolically,

$$\hat{H}_3 = S^{-1} \hat{H}_2 S, \quad (\text{A4})$$

where

$$\hat{H}_3 = \begin{bmatrix} 0 & t'_1 & 0 & 0 & \cdots \\ t'_1 & 0 & t'_2 & 0 & \cdots \\ 0 & t'_2 & 0 & t'_1 & \cdots \\ 0 & 0 & t'_1 & 0 & \ddots \\ \vdots & \vdots & \vdots & \ddots & \ddots \end{bmatrix}_{2N \times 2N}, \quad (\text{A5})$$

and S is a diagonal matrix with

$$S = \bigoplus_n S_n, S_n \equiv \beta^{n-1} \begin{bmatrix} 1 & 0 \\ 0 & \beta \end{bmatrix}. \quad (\text{A6})$$

Here the parameter is $\beta = \sqrt{(t_1 - \gamma/2)/(t_1 + \gamma/2)}$, $t'_1 = (t_1^2 - \gamma^4/4)^{1/2}$, $t'_2 = t_2$. Since the spin rotation and similarity transformation does not change eigenvalues, then \hat{H}_1 , \hat{H}_2 , and \hat{H}_3 share the same eigenspectrum. Thus, for an eigenstate $|\Psi_3\rangle = (\psi_{1,A}, \psi_{1,B}, \dots, \psi_{N,A}, \psi_{N,B})^T$ of \hat{H}_3 , there are corresponding eigenstate $|\Psi_2\rangle = S|\Psi_3\rangle$ of \hat{H}_2 and $|\Psi_1\rangle = \mathcal{R}|\Psi_2\rangle$ of \hat{H}_1 both exponentially localized at an end of the chain when $\gamma \neq 0$, namely, features the non-Hermitian skin effect. The Hamiltonian of another related quantum walk model in Ref. [7] is

$$\hat{H}_4 = \hat{H}_3 + \frac{i\gamma}{2} \bigoplus_n \sigma_z^n - \frac{i\gamma}{2} I_{2N \times 2N}. \quad (\text{A7})$$

This model does not have edge burst phenomenon due to the lack of non-Hermitian skin effect.

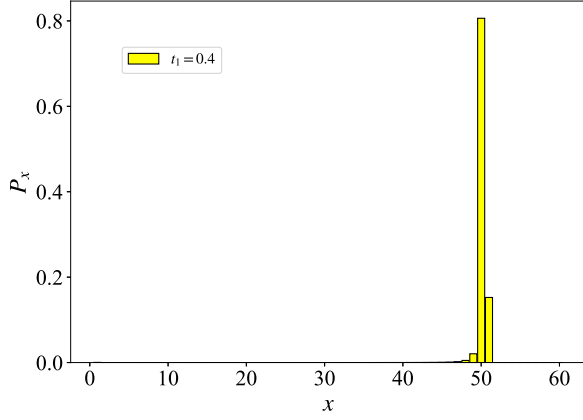


FIG. 6. The spatially resolved loss probability P_x for a walker initialized at sublattice B of site 50. Other parameters are the same as those in Fig. 2(a).

APPENDIX B: PROOF OF WAVE FUNCTION REAL-IMAGINARY PROPERTY

In Appendix B, we prove that $\psi_x^A(t)$ are real and $\psi_x^B(t)$ are purely imaginary under the initial condition $\psi_x^A(0) = \delta_{x,x_0}$, $\psi_x^B(0) = 0$. Since $\psi_x^s(t) = e^{-iE_x^s t} c_x^s(t)$ and $e^{-iE_x^s t}$ is real, we only need to consider $c_x^s(t)$ and the recursion equation is

$$i \frac{dc_x^s(t)}{dt} = \sum_{x's'} H'_{xs,x's'} c_{x'}^{s'}(t) e^{i(E_x^s - E_{x'}^{s'})t}. \quad (\text{B1})$$

The l th order recursion perturbation equation is

$$\frac{dc_x^{s(l)}}{dt} = -i \sum_{x's'} H'_{xs,x's'} c_{x'}^{s'(l-1)} e^{i(E_x^s - E_{x'}^{s'})t}. \quad (\text{B2})$$

For $l = 0$, we have $c_x^A = \delta_{x,x_0}$, $c_x^B = 0$ and the first-order perturbation $c_x^{s(1)}$ can be acquired from Eq. (B2). We note that $c_{x\pm 1}^{A(1)}$ are real and $c_{x\pm 1}^{B(1)}$, $c_x^{B(1)}$ are imaginary. If we suppose all nonzero $c_x^{A(l-1)}$ are real and $c_x^{B(l-1)}$ are imaginary, the $c_x^{A(l)}$ then can be deduced to be real. The argument is as follows, the matrix elements $H'_{xA,x'A}$ are imaginary and $H'_{xA,x'B}$ are real, the combination $-H'_{xs,x's'} c_{x'}^{s'(l-1)} e^{i(E_x^s - E_{x'}^{s'})t}$ thus is always real. From Eq. (B2), we conclude that $c_x^{A(l)}$ are real. Adding all perturbation orders of $c_x^{A(l)}$ together, we have

$$c_x^A = c_x^{A(0)} + c_x^{A(1)} + \dots + c_x^{A(l)} + \dots. \quad (\text{B3})$$

Thus, $\psi_x^A(t)$ is proved to be real. We can also prove $\psi_x^B(t)$ are purely imaginary by a similar procedure.

APPENDIX C: EFFECT OF INITIAL SITE ON EDGE BURST

In the main part of the paper, we only discussed the case where the walker was initially put at some sublattice A. We note that such initial condition is crucial for the formation of the edge burst. For the case where the walker starts from some sublattice B, the edge burst is missing even though the system features NHSE and the imaginary gap closing condition.

As a simple example, we showed this phenomenon in Fig. 6, where the system shares the same parameters as those

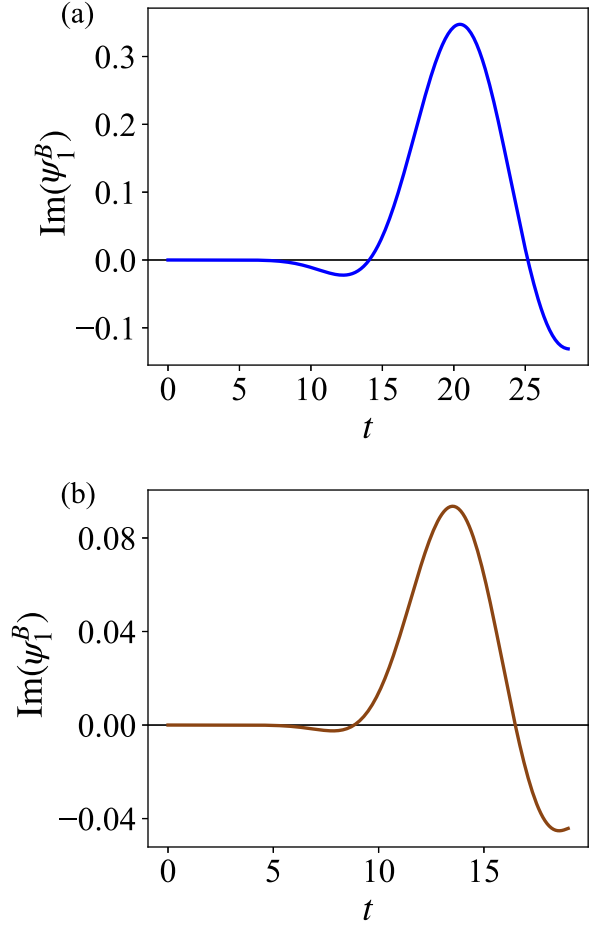


FIG. 7. Panels (a) and (b) are the edge wave functions $\psi_1^B(t)$ with perturbation calculation up to 56th order. The parameters are $\gamma_x = 0.2x$, $t_1 = 0.4$, $t_2 = 0.5$ for panel (a) and $\gamma_x = 0.2x$, $t_1 = 0.8$, $t_2 = 0.5$.

in Fig. 2(a) except that the walker is initialized at sublattice B of site 50. The dissipation probability of site B_1 is negligible small in this case due to the fast dissipation process at the initial site B_{50} , which can be verified by our time-perturbation analysis. Such result is consistent with the fact that the solution of the dynamical equation (1) depends heavily on the initial condition.

APPENDIX D: WAVE FUNCTIONS OF QUANTUM WALK WITH A NONUNIFORM LOSS RATE

In Appendix D, we give details of calculation about the wave functions of the quantum walk with a nonuniform loss rate via time-dependent perturbation theory. For simplicity, the nonuniform loss rate takes the linear form $\gamma_x = x\gamma_0$. Similar to the uniform loss rate case, we can apply our analytical method to this different class of problems. By choosing the onsite potential operator as the unperturbed Hamiltonian \hat{H}_0 , the matrix elements under the real-space representation are $\langle x, s | \hat{H}_0 | x', s' \rangle = -\frac{ix\gamma}{2} \delta_{xx'} \delta_{ss'} [1 - (\sigma_z)_{ss'}]$, with x, x' referring to the location of the unit cell and $s, s' = A, B$ referring to the sublattice label. The hopping of the walker is treated as the perturbation operator \hat{H}' and its matrix

elements are $H'_{xs,x's'} = \langle x, s | \hat{H}' | x', s' \rangle$. Then, we can use the perturbation procedure introduced in Sec. III and evaluate the real-space wave functions. For example, we evaluate the case where the system size $L = 12$ with the walker initially prepared on sublattice A of the eighth site, as shown in

Fig. 7. The analytical results are in agreement with numerical ones.

The above example shows that we can apply the non-Hermitian time-dependent theory to the systems without discrete translational symmetry.

-
- [1] R. Shankar, *Principles of Quantum Mechanics* (Springer, New York, 2012).
- [2] R. El-Ganainy, K. G. Makris, M. Khajavikhan, Z. H. Musslimani, S. Rotter, and D. N. Christodoulides, *Nat. Phys.* **14**, 11 (2018).
- [3] Y. Ashida, Z. Gong, and M. Ueda, *Adv. Phys.* **69**, 249 (2020).
- [4] K. G. Makris, R. El-Ganainy, D. N. Christodoulides, and Z. H. Musslimani, *Phys. Rev. Lett.* **100**, 103904 (2008).
- [5] S. Klaiman, U. Günther, and N. Moiseyev, *Phys. Rev. Lett.* **101**, 080402 (2008).
- [6] A. Guo, G. J. Salamo, D. Duchesne, R. Morandotti, M. Volatier-Ravat, V. Aimez, G. A. Siviloglou, and D. N. Christodoulides, *Phys. Rev. Lett.* **103**, 093902 (2009).
- [7] M. S. Rudner and L. S. Levitov, *Phys. Rev. Lett.* **102**, 065703 (2009).
- [8] S. Longhi, *Phys. Rev. Lett.* **103**, 123601 (2009).
- [9] Y. D. Chong, L. Ge, and A. D. Stone, *Phys. Rev. Lett.* **106**, 093902 (2011).
- [10] A. Regensburger, C. Bersch, M.-A. Miri, G. Onishchukov, D. N. Christodoulides, and U. Peschel, *Nature (London)* **488**, 167 (2012).
- [11] S. Bittner, B. Dietz, U. Günther, H. L. Harney, M. Miski-Oglu, A. Richter, and F. Schäfer, *Phys. Rev. Lett.* **108**, 024101 (2012).
- [12] M. Liertzer, L. Ge, A. Cerjan, A. D. Stone, H. E. Türeci, and S. Rotter, *Phys. Rev. Lett.* **108**, 173901 (2012).
- [13] L. Feng, Z. J. Wong, R.-M. Ma, Y. Wang, and X. Zhang, *Science* **346**, 972 (2014).
- [14] H. Hodaei, M.-A. Miri, M. Heinrich, D. N. Christodoulides, and M. Khajavikhan, *Science* **346**, 975 (2014).
- [15] H. J. Carmichael, *Phys. Rev. Lett.* **70**, 2273 (1993).
- [16] I. Rotter, *J. Phys. A: Math. Theor.* **42**, 153001 (2009).
- [17] Y. Choi, S. Kang, S. Lim, W. Kim, J.-R. Kim, J.-H. Lee, and K. An, *Phys. Rev. Lett.* **104**, 153601 (2010).
- [18] Z. Lin, H. Ramezani, T. Eichelkraut, T. Kottos, H. Cao, and D. N. Christodoulides, *Phys. Rev. Lett.* **106**, 213901 (2011).
- [19] T. E. Lee and C.-K. Chan, *Phys. Rev. X* **4**, 041001 (2014).
- [20] S. Malzard, C. Poli, and H. Schomerus, *Phys. Rev. Lett.* **115**, 200402 (2015).
- [21] K. Yamamoto, M. Nakagawa, K. Adachi, K. Takasan, M. Ueda, and N. Kawakami, *Phys. Rev. Lett.* **123**, 123601 (2019).
- [22] J. Li, A. K. Harter, J. Liu, L. de Melo, Y. N. Joglekar, and L. Luo, *Nat. Commun.* **10**, 1 (2019).
- [23] A. A. Zyuzin and A. Y. Zyuzin, *Phys. Rev. B* **97**, 041203(R) (2018).
- [24] H. Shen and L. Fu, *Phys. Rev. Lett.* **121**, 026403 (2018).
- [25] T. Yoshida, R. Peters, and N. Kawakami, *Phys. Rev. B* **98**, 035141 (2018).
- [26] H. Zhou, C. Peng, Y. Yoon, C. W. Hsu, K. A. Nelson, L. Fu, J. D. Joannopoulos, M. Soljačić, and B. Zhen, *Science* **359**, 1009 (2018).
- [27] M. Papaj, H. Isobe, and L. Fu, *Phys. Rev. B* **99**, 201107(R) (2019).
- [28] K. Kimura, T. Yoshida, and N. Kawakami, *Phys. Rev. B* **100**, 115124 (2019).
- [29] T. E. Lee, *Phys. Rev. Lett.* **116**, 133903 (2016).
- [30] D. Leykam, K. Y. Bliokh, C. Huang, Y. D. Chong, and F. Nori, *Phys. Rev. Lett.* **118**, 040401 (2017).
- [31] Z. Gong, Y. Ashida, K. Kawabata, K. Takasan, S. Higashikawa, and M. Ueda, *Phys. Rev. X* **8**, 031079 (2018).
- [32] H. Shen, B. Zhen, and L. Fu, *Phys. Rev. Lett.* **120**, 146402 (2018).
- [33] F. K. Kunst, E. Edvardsson, J. C. Budich, and E. J. Bergholtz, *Phys. Rev. Lett.* **121**, 026808 (2018).
- [34] S. Yao, F. Song, and Z. Wang, *Phys. Rev. Lett.* **121**, 136802 (2018).
- [35] S. Yao and Z. Wang, *Phys. Rev. Lett.* **121**, 086803 (2018).
- [36] V. M. Martinez Alvarez, J. E. Barrios Vargas, and L. E. F. Foa Torres, *Phys. Rev. B* **97**, 121401(R) (2018).
- [37] C. H. Lee and R. Thomale, *Phys. Rev. B* **99**, 201103(R) (2019).
- [38] C. H. Lee, L. Li, and J. Gong, *Phys. Rev. Lett.* **123**, 016805 (2019).
- [39] S. Longhi, *Phys. Rev. Res.* **1**, 023013 (2019).
- [40] H. Zhou and J. Y. Lee, *Phys. Rev. B* **99**, 235112 (2019).
- [41] C.-H. Liu, H. Jiang, and S. Chen, *Phys. Rev. B* **99**, 125103 (2019).
- [42] E. Edvardsson, F. K. Kunst, and E. J. Bergholtz, *Phys. Rev. B* **99**, 081302(R) (2019).
- [43] F. Song, S. Yao, and Z. Wang, *Phys. Rev. Lett.* **123**, 246801 (2019).
- [44] F. Song, S. Yao, and Z. Wang, *Phys. Rev. Lett.* **123**, 170401 (2019).
- [45] K. Yokomizo and S. Murakami, *Phys. Rev. Lett.* **123**, 066404 (2019).
- [46] K. L. Zhang, H. C. Wu, L. Jin, and Z. Song, *Phys. Rev. B* **100**, 045141 (2019).
- [47] L. Jin and Z. Song, *Phys. Rev. B* **99**, 081103(R) (2019).
- [48] T. Liu, Y.-R. Zhang, Q. Ai, Z. Gong, K. Kawabata, M. Ueda, and F. Nori, *Phys. Rev. Lett.* **122**, 076801 (2019).
- [49] A. Ghatak and T. Das, *J. Phys.: Condens. Matter* **31**, 263001 (2019).
- [50] K. Kawabata, K. Shiozaki, M. Ueda, and M. Sato, *Phys. Rev. X* **9**, 041015 (2019).
- [51] L. Herviou, J. H. Bardarson, and N. Regnault, *Phys. Rev. A* **99**, 052118 (2019).
- [52] D. S. Borgnia, A. J. Kruchkov, and R.-J. Slager, *Phys. Rev. Lett.* **124**, 056802 (2020).
- [53] S. Longhi, *Opt. Lett.* **44**, 5804 (2019).
- [54] F. K. Kunst and V. Dwivedi, *Phys. Rev. B* **99**, 245116 (2019).
- [55] K.-I. Imura and Y. Takane, *Phys. Rev. B* **100**, 165430 (2019).
- [56] N. Okuma and M. Sato, *Phys. Rev. Lett.* **123**, 097701 (2019).

- [57] J. Y. Lee, J. Ahn, H. Zhou, and A. Vishwanath, *Phys. Rev. Lett.* **123**, 206404 (2019).
- [58] S. Longhi, *Phys. Rev. Lett.* **122**, 237601 (2019).
- [59] N. Okuma, K. Kawabata, K. Shiozaki, and M. Sato, *Phys. Rev. Lett.* **124**, 086801 (2020).
- [60] Y. Yi and Z. Yang, *Phys. Rev. Lett.* **125**, 186802 (2020).
- [61] K. Kawabata, M. Sato, and K. Shiozaki, *Phys. Rev. B* **102**, 205118 (2020).
- [62] X. Zhang and J. Gong, *Phys. Rev. B* **101**, 045415 (2020).
- [63] K. Kawabata, N. Okuma, and M. Sato, *Phys. Rev. B* **101**, 195147 (2020).
- [64] S. Longhi, *Phys. Rev. Lett.* **124**, 066602 (2020).
- [65] K. Zhang, Z. Yang, and C. Fang, *Phys. Rev. Lett.* **125**, 126402 (2020).
- [66] Z. Yang, K. Zhang, C. Fang, and J. Hu, *Phys. Rev. Lett.* **125**, 226402 (2020).
- [67] N. Matsumoto, K. Kawabata, Y. Ashida, S. Furukawa, and M. Ueda, *Phys. Rev. Lett.* **125**, 260601 (2020).
- [68] C. H. Lee and S. Longhi, *Commun. Phys.* **3**, 147 (2020).
- [69] L. Li, C. H. Lee, S. Mu, and J. Gong, *Nat. Commun.* **11**, 1 (2020).
- [70] Y. Fu, J. Hu, and S. Wan, *Phys. Rev. B* **103**, 045420 (2021).
- [71] R. Okugawa, R. Takahashi, and K. Yokomizo, *Phys. Rev. B* **102**, 241202(R) (2020).
- [72] S. Longhi, *Phys. Rev. B* **102**, 201103(R) (2020).
- [73] C.-H. Liu, K. Zhang, Z. Yang, and S. Chen, *Phys. Rev. Res.* **2**, 043167 (2020).
- [74] E. Edvardsson, F. K. Kunst, T. Yoshida, and E. J. Bergholtz, *Phys. Rev. Res.* **2**, 043046 (2020).
- [75] P. Gao, M. Willatzen, and J. Christensen, *Phys. Rev. Lett.* **125**, 206402 (2020).
- [76] L. Xiao, T. Deng, K. Wang, G. Zhu, Z. Wang, W. Yi, and P. Xue, *Nat. Phys.* **16**, 761 (2020).
- [77] A. Ghatak, M. Brandenbourger, J. Van Wezel, and C. Coulais, *Proc. Natl. Acad. Sci. USA* **117**, 29561 (2020).
- [78] T. Helbig, T. Hofmann, S. Imhof, M. Abdelghany, T. Kiessling, L. Molenkamp, C. Lee, A. Szameit, M. Greiter, and R. Thomale, *Nat. Phys.* **16**, 747 (2020).
- [79] T. Hofmann, T. Helbig, F. Schindler, N. Salgo, M. Brzezińska, M. Greiter, T. Kiessling, D. Wolf, A. Vollhardt, A. Kabaši, C. H. Lee, A. Bilušić, R. Thomale, and T. Neupert, *Phys. Rev. Res.* **2**, 023265 (2020).
- [80] S. Weidemann, M. Kremer, T. Helbig, T. Hofmann, A. Stegmaier, M. Greiter, R. Thomale, and A. Szameit, *Science* **368**, 311 (2020).
- [81] Y. Song, W. Liu, L. Zheng, Y. Zhang, B. Wang, and P. Lu, *Phys. Rev. Appl.* **14**, 064076 (2020).
- [82] L. E. F. F. Torres, *JPhys Mater.* **3**, 014002 (2020).
- [83] E. J. Bergholtz, J. C. Budich, and F. K. Kunst, *Rev. Mod. Phys.* **93**, 015005 (2021).
- [84] L. Wang, Q. Liu, and Y. Zhang, *Chin. Phys. B* **30**, 020506 (2021).
- [85] H. Hu and E. Zhao, *Phys. Rev. Lett.* **126**, 010401 (2021).
- [86] K. Yokomizo and S. Murakami, *Phys. Rev. B* **103**, 165123 (2021).
- [87] N. Okuma and M. Sato, *Phys. Rev. B* **103**, 085428 (2021).
- [88] H.-G. Zirnstein, G. Refael, and B. Rosenow, *Phys. Rev. Lett.* **126**, 216407 (2021).
- [89] J. Claes and T. L. Hughes, *Phys. Rev. B* **103**, L140201 (2021).
- [90] N. Okuma and M. Sato, *Phys. Rev. Lett.* **126**, 176601 (2021).
- [91] K. Kawabata, K. Shiozaki, and S. Ryu, *Phys. Rev. Lett.* **126**, 216405 (2021).
- [92] C.-X. Guo, C.-H. Liu, X.-M. Zhao, Y. Liu, and S. Chen, *Phys. Rev. Lett.* **127**, 116801 (2021).
- [93] X.-Q. Sun, P. Zhu, and T. L. Hughes, *Phys. Rev. Lett.* **127**, 066401 (2021).
- [94] T. Haga, M. Nakagawa, R. Hamazaki, and M. Ueda, *Phys. Rev. Lett.* **127**, 070402 (2021).
- [95] K. Wang, A. Dutt, K. Y. Yang, C. C. Wojcik, J. Vučković, and S. Fan, *Science* **371**, 1240 (2021).
- [96] W.-T. Xue, M.-R. Li, Y.-M. Hu, F. Song, and Z. Wang, *Phys. Rev. B* **103**, L241408 (2021).
- [97] R. Okugawa, R. Takahashi, and K. Yokomizo, *Phys. Rev. B* **103**, 205205 (2021).
- [98] Z. Lin, L. Ding, S. Ke, and X. Li, *Opt. Lett.* **46**, 3512 (2021).
- [99] S. Longhi, *Opt. Lett.* **46**, 4470 (2021).
- [100] K. Yokomizo and S. Murakami, *Phys. Rev. B* **104**, 165117 (2021).
- [101] S. Longhi, *Phys. Rev. B* **104**, 125109 (2021).
- [102] K. Wang, A. Dutt, C. C. Wojcik, and S. Fan, *Nature (London)* **598**, 59 (2021).
- [103] K. Wang, T. Li, L. Xiao, Y. Han, W. Yi, and P. Xue, *Phys. Rev. Lett.* **127**, 270602 (2021).
- [104] K. Zhang, Z. Yang, and C. Fang, *Nat. Commun.* **13**, 1 (2022).
- [105] D. Wu, J. Xie, Y. Zhou, and J. An, *Phys. Rev. B* **105**, 045422 (2022).
- [106] S. Weidemann, M. Kremer, S. Longhi, and A. Szameit, *Nature (London)* **601**, 354 (2022).
- [107] Q. Lin, T. Li, L. Xiao, K. Wang, W. Yi, and P. Xue, *Phys. Rev. Lett.* **129**, 113601 (2022).
- [108] S. Longhi, *Phys. Rev. Lett.* **128**, 157601 (2022).
- [109] W. N. Faugno and T. Ozawa, *Phys. Rev. Lett.* **129**, 180401 (2022).
- [110] Y. Li, C. Liang, C. Wang, C. Lu, and Y.-C. Liu, *Phys. Rev. Lett.* **128**, 223903 (2022).
- [111] W. Zhu and J. Gong, *Phys. Rev. B* **106**, 035425 (2022).
- [112] V. Mittal, A. Raj, S. Dey, and S. K. Goyal, *Sci. Rep.* **11**, 10262 (2021).
- [113] C. Wu, A. Fan, and S.-D. Liang, *AAPPS Bull.* **32**, 39 (2022).
- [114] O. Sigwarth and C. Miniatura, *AAPPS Bull.* **32**, 23 (2022).
- [115] Z.-H. Xu, X. Xia, and S. Chen, *Sci. China: Phys. Mech. Astron.* **65**, 227211 (2022).
- [116] W.-T. Xue, Y.-M. Hu, F. Song, and Z. Wang, *Phys. Rev. Lett.* **128**, 120401 (2022).
- [117] L. Xiao, W.-T. Xue, F. Song, Y.-M. Hu, W. Yi, Z. Wang, and P. Xue, *arXiv:2303.12831*.
- [118] C. Yuce and H. Ramezani, *Phys. Rev. B* **107**, L140302 (2023).